NDT&E International 160 (2026) 103667

Contents lists available at ScienceDirect

NDT and E International

journal homepage: www.elsevier.com/locate/ndteint

Effective damage detection method based on electromechanical impedance and parallel connection of the transducers

Shishir Kumar Singh [a,b,*], Paweł H. Malinowski [a]

[a] Institute of Fluid Flow Machinery, Polish Academy of Sciences, Fiszera 14, 80-231, Gdansk, Poland
[b] Department of Aerospace Structures and Materials, Delft University of Technology, Kluyverweg 1, Delft, 2629 HS, the Netherlands

ARTICLE INFO

Keywords:
Electromechanical impedance
Piezoelectric
Sensor fusion
parallel combination
Damage index
Damage detection

ABSTRACT

Several research studies aim to employ the electromechanical impedance method (EMI) for effective health monitoring. At the same time, limited studies focused on increasing damage detection efficiency using a combination of sensors under noise and temperature variation. This novel research aims to outperform the temperature compensation algorithm development by using a robust multiple-sensor instrumentational strategy for damage detection in structures. This research combines EMI resistance data in parallel connection for damage detection in the steel beam structure. The resistance parameters based on parallel combinations are studied and compared with the output of single transducers or series connections for the added simulated mass, and simulated cracks with variations of the temperature conditions. The performance comparison has been made in the selected frequency range of 1–100 kHz for the additional mass and 30-80 kHz for the simulated cracked steel beam. The damage sensitivity-based performance comparison has been studied using the root mean square deviation (RMSD) index. The resistance data fusion-based parallel connection has shown a better performance of damage detection capability over a single actuator or a series of connected actuators in varying environmental temperature conditions for the real crack and simulated added mass. The simulated added mass and crack are successfully detected at a higher temperature in the case of the parallel combination of the actuators.

1. Introduction

Data collection in continuous structural health monitoring (SHM) employing a sensor network can be time-consuming, resulting in an extensive amount of data that needs to be stored and processed. Among the various SHM techniques, the most popular are guided (Lamb) wave propagation and electromechanical impedance. Both of them often employ piezoelectric transducers, because they can work both as actuators and sensors due to the converse and direct piezoelectric effect. The popular piezoelectric material used is Lead Zirconate Titanate (PZT) due to its strong electromechanical coupling properties and stability. The electromechanical impedance (EMI) technique is an efficient structural monitoring tool in mechanical, aerospace, and civil structures. In this method, piezoelectric transducers excite the investigated structure and sense the response, from which the structural condition is inferred. Damage assessment is based on variations in the electrical quantities (impedance, resistance, conductance, and others) as a function of frequency, and comparing the responses at different structural conditions [1]. For example, Wu et al. reported bolted connection monitoring using an instrumented wearable piezoelectric ring device, where the resonance peaks at specific frequencies in the EMI spectrum decreased as the bolt torque decreased [2]. The EMI approach utilizes a high-frequency range to assess local structural health, as it is sensitive to early cracks, delamination, and other structural defects [3,4]. However, the technique often results in a laborious data retrieval process, a large amount of data, and the need to select an effective frequency range. To address these limitations, several researchers have explored sensor configurations and data fusion techniques to improve the sensitivity and efficiency of EMI-based damage detection. Luo et al. aimed to achieve diverse EMI properties by describing a basic sensor architecture [5]. The authors used the multi-sensing EMI system to connect four smart modulation transducers with more than one magnetic disk thickness in series. Zuo et al. developed a modified EMI technique for crack detection that involves fusing information from multiple sensors using a new damage-sensitive feature to examine the degree and position of crack damage in a pipeline [6]. Adhikari et al. introduced a modified dual piezo arrangement in which responsiveness improves with the quantity of actuators linked in parallel as the output current rises, which allows

* Corresponding author. Institute of Fluid Flow Machinery, Polish Academy of Sciences, Fiszera 14, 80-231, Gdansk, Poland.
E-mail address: s.k.singh@tudelft.nl (S.K. Singh).

https://doi.org/10.1016/j.ndteint.2026.103667
Received 6 August 2025; Received in revised form 9 January 2026; Accepted 3 February 2026
Available online 3 February 2026

for early damage identification and enhanced severity evaluation for reinforced concrete (RC) structures [7]. Chen et al. evaluated bolt looseness utilizing series and parallel connections. They employed smart washers in series to obtain an impedance signal in a single sweep [8]. Shishir et al. report the use of two piezoelectric transducers on a steel beam structure to quantify damage. A theoretical approach for modeling serial and parallel connections was devised and tested, and was demonstrated in the case of a steel beam with an added mass at a specific temperature [9].

Other studies, such as those by Priya et al. [10] and Balamonica et al. [11], used multi-sensing EMI approaches for concrete strength monitoring due to improper curing to enhance data retrieval speed through independent and multiplexed sensor patches. The authors have analyzed the embedded sensor's conductance data using damage metrics of root mean square deviation (RMSD), mean absolute percentage deviation (MAPD), and correlation coefficient (CC) [10]. However, while previous research primarily focused on speeding up the data collection process, less attention was paid to robust damage detection under changing conditions, such as noise presence or temperature fluctuations.

Extensive experimental studies have explored the impact of temperature on PZT materials and structural behavior. These studies have shown that temperature changes can produce effects similar to those caused by structural damage [12,13]. Temperature variations affect the real part of impedance (resistance), and horizontal shifts are observed. These effects are more pronounced in the high-frequency range of impedance measurements [14,15]. A wide range of theoretical and experimental research has focused on developing algorithms for temperature compensation using the cross-correlation compensation method [14,16]. Recent studies have sought to mitigate these challenges using artificial intelligence. For instance, integration of EMI data with deep learning models such as one-dimensional convolutional neural networks (1D-CNNs) has improved automatic identification and quantification of small-scale damage in reinforced concrete, enhancing accuracy and computational efficiency [17,18]. EMI-based monitoring has also been extended to carbon-fiber-reinforced polymer (CFRP) retrofitted beam–column joints (BCJs) and fiber-reinforced concrete (FRC) structures using statistical indices such as RMSD and hierarchical clustering analysis (HCA) for load-induced damage detection [19,20]. These advancements collectively strengthen the reliability and real-time applicability of EMI-based SHM systems. Despite these advances, only a few measurement-based, robust data fusion strategies have been proposed to mitigate the influence of temperature variation on damage identification.

Nevertheless, a clear knowledge gap remains in developing measurement-based, low-complexity fusion strategies that can effectively suppress temperature and noise interference while preserving the EMI method's high sensitivity. The results of the specific multi-sensing approach with parallel or serially connected transducers under varying temperature conditions have not yet been demonstrated. This work discusses the advantage of the parallel combination of transducers for measuring the resistance to detect damage under temperature and noise influence. The EMI method is local and sensitive to the area around the piezoelectric sensor. Joining two sensors allows for extending the sensitivity range, because the output is a combined response of two sensors. Unlike conventional approximation or compensation techniques, which primarily correct temperature-induced signal shifts using mathematical modeling. However, their accuracy depends strongly on extensive baseline data and consistent temperature–impedance correlations [21,22]. However, their accuracy strongly depends on extensive baseline data and reliable temperature and impedance correlation; our approach reduces their influence at the measurement level itself by combining sensor responses.

The temperature sensitivity was studied and implemented with an experimental EMI resistance signal of the structure in a limited temperature variation. The setup has been realized for the multi-input and single-input series and parallel connections to fuse signals for the resistance data. The damage evaluations using fused resistance demonstrated the benefit of using a parallel connection compared to other arrangements and were tested on the steel beam with extra weight. In this study, the authors find that series combinations of the resistance are prone to noise and temperature variation and show fewer percentage changes with respect to baseline signals. The method uses two sensors operating in tandem to lessen the impact of temperature change using resistance fusion. The mass was detected using fused parallel resistance, and the measuring time was reduced by half as well. Five damage scenarios were examined, two involving temperature changes by comparing series, parallel connections, and individual setups. The paper investigated the statistical RMSD damage index for the simulated additional mass and simulated cracks on steel beams under low-temperature fluctuation for robust damage detection. We propose to use the traditional RMSD metric, but enhance the EMI sensitivity by connecting the used piezoelectric sensors. The common advantage of using such metrics is straightforward calculation, where the unknown case (possibly damaged) is compared with data for known healthy (undamaged) cases. A successful example of using smart aggregate EMI sensors for concrete and employing the RMSD index was reported in Refs. [23,24].

2. Theory and methodology

In this work, the damage evaluation on the steel beam structure is realized by the EMI method that employs PZT sensors. In the EMI technique, the bonded PZT acts simultaneously as an actuator and a sensor. When a voltage is applied, the PZT induces local vibrations in the host structure. The electromechanical coupling causes the electrical impedance ($Z(\omega)$) of the PZT to depend on the mechanical impedance of the structure ($Z_s(\omega)$). The electrical impedance ($Z(\omega)$) of the bonded PZT transducer depends on the mechanical impedance of the structure (Z_s), and in the 1D case, can be calculated using Eq. (1) [25,26]. The impedance $Z(\omega)$) is a function of resistance ($R(\omega)$) and reactance ($X(\omega)$), Any change in the stiffness, mass, or damping of the structure modifies Z_s, and hence the coupled electrical ($Z(\omega)$), ($R(\omega)$), and ($X(\omega)$) measured at the PZT terminals. Eq. (1) applies to PZT sensors of different sizes and shapes by substituting their respective geometric (radius, width, or thickness) and material parameters.

$$Z(\omega)=\frac{V}{I}=\frac{h_p}{j\omega\bar{\varepsilon}_{33}^{T}\pi a^2}\left[1-\frac{2{d_{31}}^2}{\bar{s}_{11}^{T}\bar{\varepsilon}_{33}^{T}(1-\mu)}\left[1-\frac{1}{\frac{Z_a}{Z_s}+1}\left(\frac{2}{\overline{\varphi}}\right)\left\{\frac{J_1(\overline{\varphi})}{J_0(\overline{\varphi})}\right\}\right]\right]^{-1} \tag{1}$$

where, $\bar{\varepsilon}_{33}^{T}=\varepsilon_{33}^{T}(1-j\delta)$, $\bar{s}_{11}^{E}=s_{11}^{E}(1-j\eta)$, $\overline{c_p}=1/\sqrt{\rho\bar{s}_{11}^{E}(1-\mu^2)}$, $\overline{\varphi}=\frac{\omega}{\overline{c_p}}a$, $'J_0{}'$ and $'J_1{}'$ are zero and first-order Bessel function of the first kind respectively, $'Z_a{}'$ is the short-circuited mechanical impedance of piezoelectric transducer, $'Z_s{}'$ is the mechanical impedance of the structure, $'h_p{}'$ the thickness of piezoelectric transducer, a - radius of the transducer, $'\rho'$ - density, $'s_{11}^{E}{}'$ is the compliance coefficient, $'d_{31}'$ is the piezoelectric coefficient of the transducer for direction 3-1 (electric field applied in direction 3, strains in direction-1) characterizes the electromechanical coupling behavior of piezoelectric materials, j-complex unit, ε_{33}^{T} is the complex permittivity of the piezoelectric transducer for direction 33, $'\eta'$ is the mechanical loss factor and δ is dielectric loss factor.

The selection of effective impedance peaks depends on the host material and structural characteristics. For steel structures, which have high stiffness and low damping, effective peaks typically appear at frequencies above 30 kHz [27]. For composite materials, the anisotropic nature and internal layering often result in split or multiple peaks below 150 kHz [28]. In the case of concrete structures, due to high damping and heterogeneity, the response peaks are broader and distributed within 10–250 kHz [20]. These frequency peak shifts in the impedance

spectrum are interpreted as changes in local stiffness or mechanical impedance, which are quantified using statistical indices such as the Root Mean Square Deviation (RMSD). These indices transform the raw impedance response into engineering information that reflects damage severity, location, and progression over time. For practical implementation, PZT sensors are protected to ensure long-term reliability and stability during field monitoring. They can be embedded within structural elements for durable and stable bonding [29–31] or surface-bonded and coated with protective layers such as epoxy or polyurethane to safeguard against moisture, corrosion, and mechanical wear [32]. The experimental steel beam data were collected in the 1 kHz–4 MHz frequency range, and good deviation of the healthy and damaged state data was found in resistance for frequency ranges of 1-100 kHz for the simulated added mass and 30-80 kHz for the developed cracked steel beam, respectively. For damage detection and classification, several frequency ranges with 20 to 30 peaks are often used since a larger mode density indicates a more dynamic interaction between actuators and host structures [33]. However, Singh et al. employed a novel frequency-range selection technique based on the standard deviation of the EMI frequency spectra, utilizing the maxima of the standard deviation [34,35]. The high-frequency noise is filtered using a 9th-order polynomial regression Savitzky-Golay (SG) filter, without compromising the underlying spectral characteristics [36], and detrending by eliminating frequency dependency from the contours [37].

This research focuses on the connections of the PZT transducers to enhance damage sensitivity. The coupled impedance of n connected transducers (Fig. 1) can be expressed as [38]:

$$Z_{coupled}(\omega) = R_0 + \frac{1}{j\omega C_0} + \sum_{i=1}^{n} \frac{1}{\frac{1}{R_i} + \frac{1}{j\omega L_i} + j\omega C_i} \tag{2}$$

where R_i, L_i and C_i are analogous to PZT's mechanical damping, mass, and elastic compliance, respectively, for the ith transducer. R_0 and C_0 represents resistance and capacitance, respectively [39]. The capacitance is a measure of the redistribution of electric charge that occurs as a consequence of a change in the applied voltage. The capacitance of a device measures the redistribution of the electric charge caused by a change in the applied voltage [5,38]. The PZT's resistance $R_1(\omega)$ and $R_2(\omega)$ can be obtained from Eq. (2) in the form given by Eqs. (3) and (4):

$$R_1(\omega) = R_0 + \frac{R_1\omega^2 L_1^2}{\omega^2 L_1^2 - {R_1}^2(\omega^2 L_1 C_1 - 1)^2} \tag{3}$$

$$R_2(\omega) = R_0 + \frac{R_2\omega^2 L_2^2}{\omega^2 L_2^2 - {R_2}^2(\omega^2 L_2 C_2 - 1)^2} \tag{4}$$

Further, substituting the value of $R_1(\omega)$ and $R_2(\omega)$ into Eqs. (5) and (6) yield the resultant resistance for series ($R_s(\omega)$) and parallel ($R_p(\omega)$).

$$R_s(\omega) = R_1(\omega) + R_2(\omega) \tag{5}$$

$$\frac{1}{R_p(\omega)} = \frac{1}{R_1(\omega)} + \frac{1}{R_2(\omega)} \tag{6}$$

A series connection adds resultant resistance amplitude, whereas a parallel connection reduces it, depending on the number of transducers used. The output external effect on resistance is lower when the combined signal is connected in parallel, and higher when it is connected in series. Eqs. (7) and (8) demonstrate a resultant series (R_s) and parallel (R_p) connection for the i^{th} PZTs, where R_1^i, C_1^i and L_1^i are resistance, capacitance, and inductance values, respectively, for the i^{th} PZTs.

$$R_s(\omega) = \sum_{i=1}^{2} R_0 + \frac{R_1^i\left[\omega L_1^i\right]^2}{\left[\omega L_1^i\right]^2 - \left[R_1^i\left(\omega^2 L_1^i C_1^i - 1\right)\right]^2} \tag{7}$$

$$R_p(\omega) = 1 \Big/ \sum_{i=1}^{2} 1 \Big/ \left[R_0 + \frac{R_1^i\left[\omega L_1^i\right]^2}{\left[\omega L_1^i\right]^2 - \left[R_1^i\left(\omega^2 L_1^i C_1^i - 1\right)\right]^2}\right] \tag{8}$$

The damage sensitivity is investigated using the RMSD indices of healthy and damaged EMI resistance data. Eq. (9) is used to quantify damage with a baseline healthy state of the structure, utilizing the resistance (R) data provided below [26,40]. The EMI-based damage detection approach always uses the healthy state data as the reference and calculates the damage index.

$$RMSD = \sqrt{\frac{\sum_{j=1}^{n}\left(R_{pi} - R_{pi}^o\right)^2}{\sum_{j=1}^{n}\left(R_{pi}^o\right)^2}} \tag{9}$$

where the symbol n is used for frequency spectrum samples, symbol R_{pi}^o is used for the i^{th} healthy state single sample parallel resistance spectrum, and R_{pi} is the single sample of the parallel resistance spectrum for the i^{th} damage state.

3. Experimental setup

The EMI experimental study was conducted on a steel beam size of 35.5 cm × 3 cm × 0.3 cm, with two attached piezoelectric transducers (p1 and p2). This work was designed as a laboratory-scale feasibility study; hence, a small sample was used, and two sensors were sufficient to demonstrate the effect of series and parallel connections. The rationale behind the selection of the distance between p1 and p2 sensors is guided by Singh et al. [41], who studied the damage sensitivity of a single sensor. The maximum separation between the two sensors was kept smaller than the combined maximum sensitivity range of both sensors. Four damage scenarios were considered, as illustrated in Fig. 2.

The EMI-based structural response across the PZTs terminals is measured with an impedance analyzer (model IM3570). The magnitude of excitation chosen for the experiments is 1V using a sweep sine wave signal [42]. The experiment is carried out with a surface-bonded SONOX P502 PZT transducer with a diameter of 10 mm and a thickness of 0.5 mm. Table 1 describes the electrical features of the used transducer.

Initially, three mass placement scenarios are examined in the study. Fig. 2a shows a 50-g additional mass (shown by the orange circle) placed 3 cm away from the p1 transducer, whereas Fig. 2b and c shows a 50-g and 5-g additional mass placed 3 cm away from the left side's end, respectively. To examine the sensitivity of the damage signature in the

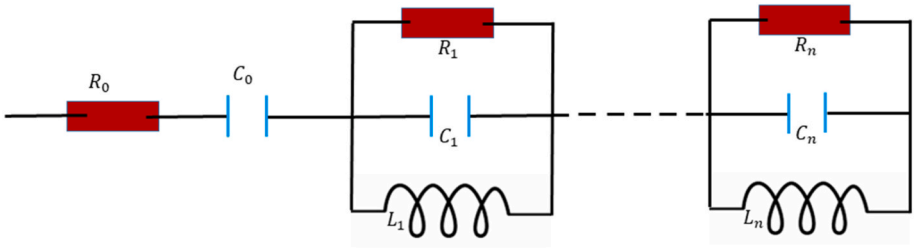

Fig. 1. Diagram of n connected transducers.

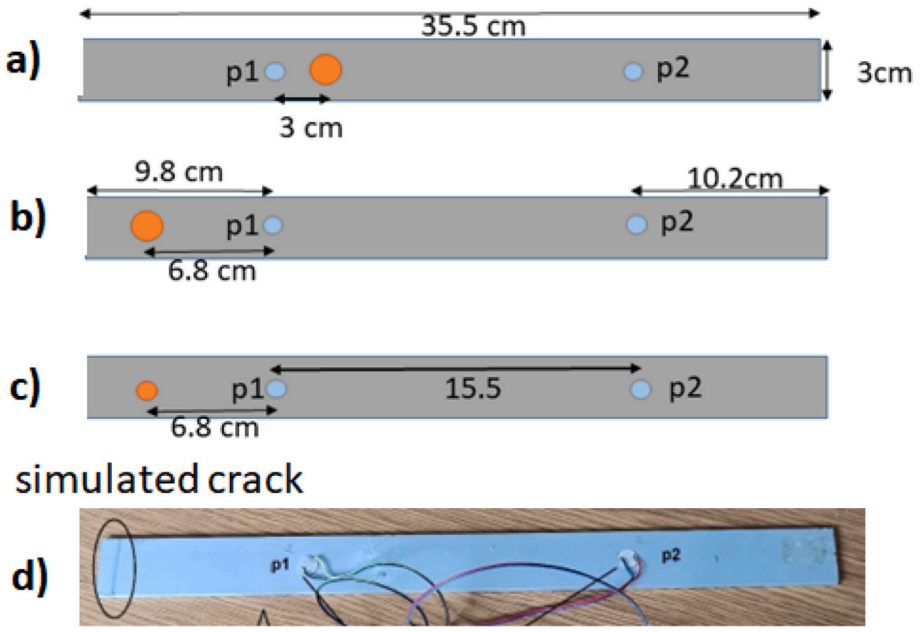

Fig. 2. Diagram of steel beam structure with different damage conditions.

Table 1
The key properties of the SONOX P502 transducer.

1	ρ	7740 kg/m3
2	s11 = s22	18.5×10^{-12} Pa^{-1}
	s33	20.7×10^{-12} Pa^{-1}
	s32 = s31	102.66×10^{-12} Pa^{-1}
	s12	52.247×10^{-12} Pa^{-1}
	s44 = s55	34×10^{-12} Pa^{-1}
	s66	67.494×10^{-12} Pa^{-1}
3	ε_{11}^T	$1950 \times \varepsilon_0$
	ε_{22}^T	$1950 \times \varepsilon_0$
	ε_{33}^T	$1850 \times \varepsilon_0$
4	δ	0.0125
5	Thermal coefficient, **α**	$\mathbf{5.2 \times 10^{-4}}$

changing environmental conditions, the temperature was raised from 19 °C to 23 °C and then to 30 °C. The three temperature conditions were intentionally selected to represent typical ambient variations observed under laboratory and field environments. The aim was to assess temperature-induced impedance shifts within practical operational limits rather than extreme conditions. The temperature of the surroundings was varied to identify the most effective connections for simulated small and large additional masses. As a fourth scenario, a saw cut is used to remove material, creating a crack at a distance of 1.2 cm from the extreme left end of the steel beam (Fig. 2d). During the saw cut process, the beam is firmly clamped in a bench vice to prevent movement and ensure precise cutting. The saw blade then removes a thin layer of material, creating a shallow notch that slightly weakens the surface and concentrates stress locally. Fig. 3 shows the experiment's setup diagram of the steel beam structure having mass (M_s), stiffness (K_s), and damping (C_s) with transducer connections. The EMI variables' data are measured with 200 Hz steps between 1 kHz and 4 MHz. The 200 Hz step size was sufficient to capture the peak shift variations relevant to damage detection in this study, as intervals smaller than 200 Hz would significantly increase measurement time. An average of fifty measurements makes up each set of measurement data for the healthy and damaged structures. In addition, to minimize the influence of ambient mechanical vibrations and electromagnetic interference, the experimental setup was mounted on a vibration-isolation platform using shielded twisted-pair cables, short lead lengths, proper grounding, and physical separation from power electronics.

4. Results and discussions

This paper demonstrates damage sensitivity for the four cases of damage scenarios based on series and parallel combinations of transducers. The connections and respective measurements were assigned with the following symbols: p1 and p2 – single transducers, p12s –series combination, and p12p – parallel combination, as indicated in Fig. 4.

The p1, p2, p12s, and p12p healthy state (symbol 'H') resistance spectra in the frequency domain are shown in Fig. 5. The method is demonstrated in the 1-100 kHz range for the simulated added mass and in the 30-80 kHz range for the produced cracked steel beam. Fig. 6 shows the few resistance data collected in this range from the individual sensors as well as the sensors in a parallel combination for investigation. In the comparative study of a single sensor and a combination of sensors, the parallel combination covers all peaks of p1 and p2, reflecting changes due to damage and temperature variation. In Fig. 6, for example, p2-H19 does not exhibit any peaks at 6.42×10^4 Hz, whereas the parallel connection (p12p-H19) and p1-H19 show peaks corresponding to the R amplitude change. The benefits of using an R data fusion parallel connection on a steel beam with additional mass and a simulated crack are proven for parallel connections proposed and tested under varying temperature conditions.

The author tries to investigate these connections under maximum 12 °C temperature variation conditions. Temperature variations can affect the electrical resistance of the materials involved in the parallel and series connections. This study reports experimental observations in a limited temperature range, with many cases studied. The damage detection investigation is split into two portions. The first section of the study covers simulated mass on the steel beam, while the second case study examines the simulated cracking as the temperature of the environment varies. There are two types of weight used, firstly, 50 g, and then 5 g, to analyze the damage sensitivity at a constant temperature. Further, the environmental temperature increased from 19 °C to 23 °C and further to 30 °C to investigate the most effective combinations towards the sensitivity to damage.

4.1. Section I: robust damage detection for varied damage severity at given environmental temperature conditions

Fig. 7 depicts the healthy and damaged state resistance (R) spectrum

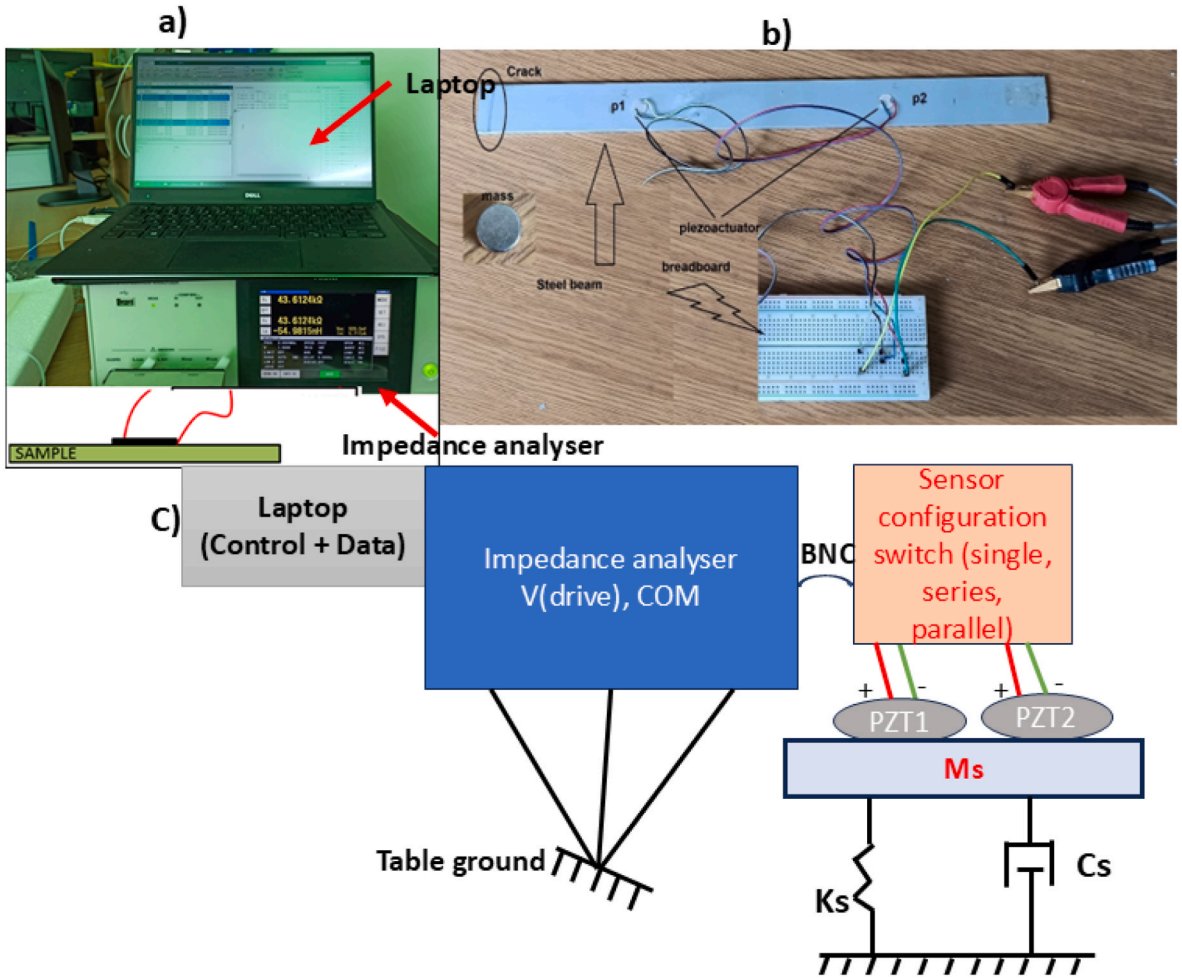

Fig. 3. Diagram showing (a) the EMI experimental setup, (b) PZT combinations on a steel beam structure for damage detection, and (c) the circuit diagram illustrating the electrical connections.

plots of the p1, p2, p12p, and p12s for the smallest mass damage scenario, as shown in Fig. 2. The damaged state exhibits anomalous behavior in the 1-100 kHz frequency range compared to healthy state data. As a result, this range is appropriate for illustrating the proposed quantitative technique for damage identification. The RMSD damage indexes of the p1, p2, p12s, and p12p connections were compared using Eq. (9). Figs. 8–10 illustrate RMSD damage sensitivity for all simulated additional mass locations in the steel beam structure. Both the directly measured unprocessed data ("raw") and the detrended filtered data ("F") were analyzed for comparison of sensor connections. They are represented by distinct surface colors, which are dark green ("raw") and light green ("F") for the healthy state, and dark red ("raw") and light red ("F") for the damaged state. All damage cases have been identified because the damage case values exceeded the healthy case values. Two repeated healthy state measurements were utilized to calculate the threshold (green bar); the difference reflects measurement errors due to noise or uncertainty. In the nomenclature, the symbols 'H' and 'M' represent the healthy and additional mass state, respectively. The p12p combination, both raw and detrended filtered (H-F and M − F) indices, shows substantial damage sensitivity with respect to a healthy steel beam structure. The p1, p2, and p12s have also shown damage detection for the simulated additional mass based on raw and filtered data. Fig. 9 shows the comparative study of these connections for healthy and damaged states in the raw and filtered conditions for the healthy and damaged conditions. The p2 exhibits greater damage detection sensitivity than the p1 based on raw data, although the damage is closer to p1, which goes against our expectations. This can be seen with the "M-raw" data damage RMSD index, because the raw measurements had noise and contained a trend. Furthermore, the calculation was performed on detrended filtered data; indeed, the RMSD value in Fig. 10 is higher for p2 than for p1. But, the ratio of damaged bars with respect to healthy bars is important, and for p1, this ratio is 5.76, and for p2, this ratio is 5.8. The noise is the reason behind it, being checked based on SG filtered data. As no data filtering was applied during experimentation, a 1 V excitation voltage was used to ensure sufficient signal strength while preventing nonlinear distortions in the impedance response. The calculated ratio for the damage bar with respect to the healthy bar for filtered data of p1 is 7.1, which is more sensitive than that of the p2 value of 3.7. In all damage cases, the damage was always discovered since the severity of the damage was always quite high and above healthy values for temperature, kept constant at 19 °C.

4.2. Section II: robust damage detection in varied environmental temperature conditions

In this part, damage is investigated for the small mass of 5 g that has a lower influence on the structure than the 50-g mass. This study fuses resistance data, and it employs two transducers working in tandem to reduce the influence of temperature changes. The combinations were investigated and compared to the output of single transducers for adding a modest 5-g simulated mass and a simulated crack with external temperature change.

Case I. A damage investigation was carried out for the small mass of 5

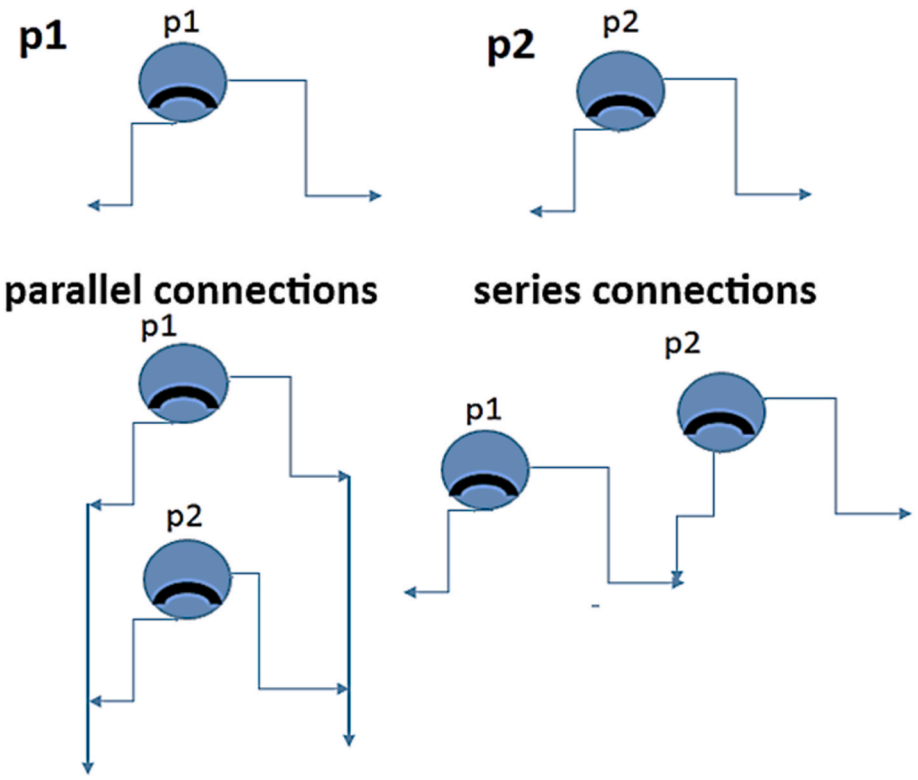

Fig. 4. The combination used for damage detection in the steel beam.

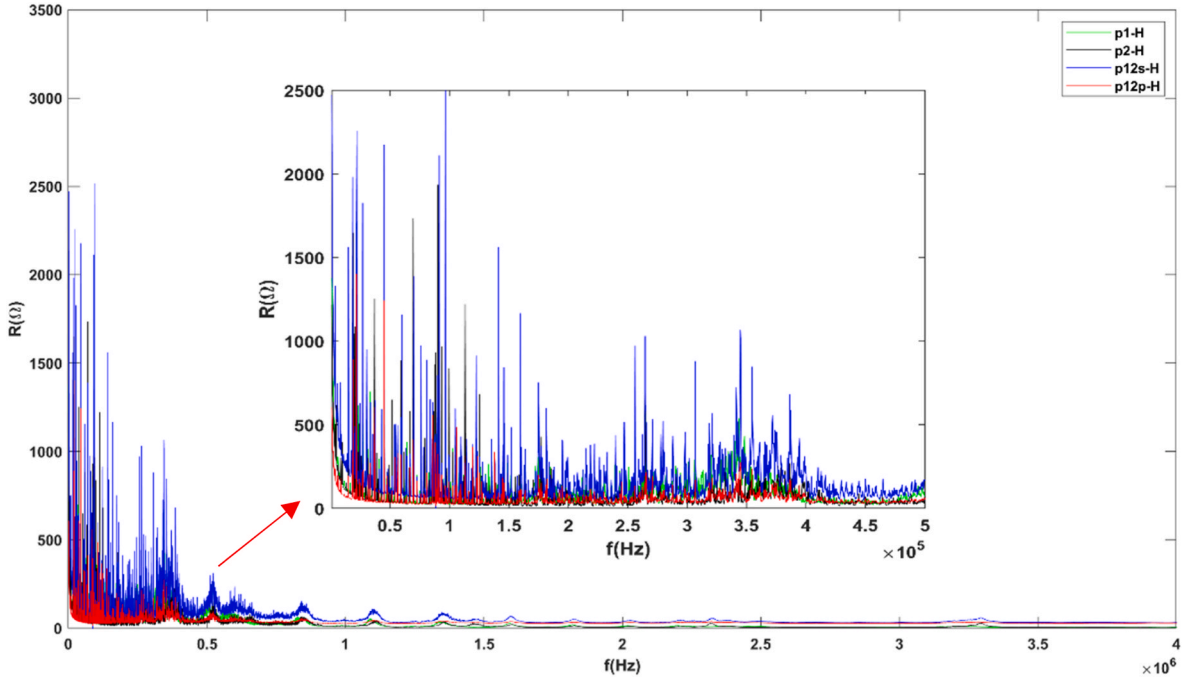

Fig. 5. The EMI resistance data in the frequency domain for the p1, p2, p12p, and p12s.

g, as indicated in Fig. 2c, on the structure under different degrees of temperature. The damage sensitivity of a steel bar was studied at the three temperatures: 19 °C, 23 °C, and 30 °C. The experimental R-values of p1, p2, p12p, and p12s are compared under varied temperature conditions to investigate the behavior of the combinations stated above. Fig. 11 displays the RMSD damage indices of healthy and damaged state EMI data. The symbols H-19, H-23, H-30, H-19/23, H-19/30, M − 19, M − 30, and M-19/30 used in Fig. 11 are explained in Table 2. The parallel connection (p12p) outperforms p1, p2, and p12s due to the smaller resultant resistance magnitude, which results in lesser susceptibility and accuracy to noises and variation in the surroundings. The p12p has the most growing damage index disparities for 5-g mass across all healthy state temperatures, H-19, H-23, and H-30. Fig. 11 illustrates a comparison of the healthy and damaged states of experimental data for the p12p

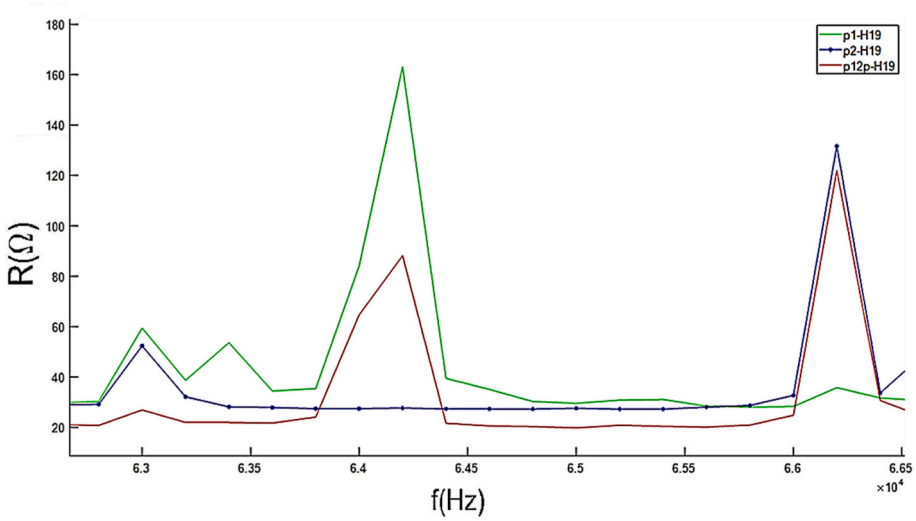

Fig. 6. Comparative R plot of healthy data for p1, p2, and p12p sensor.

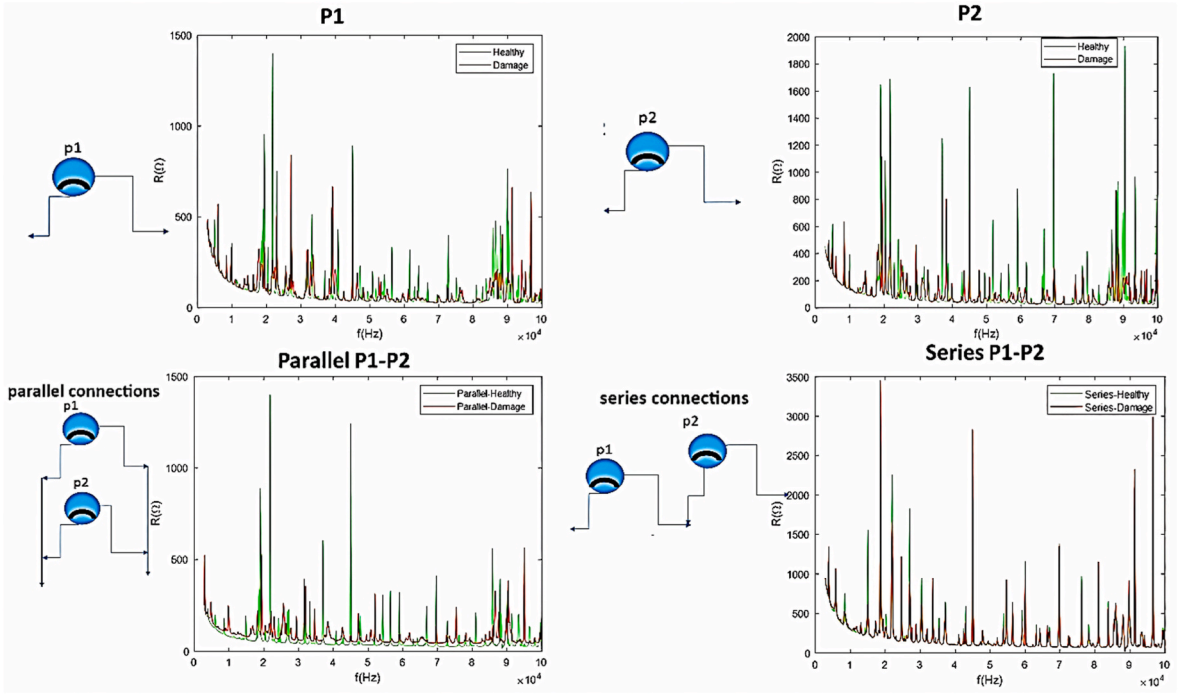

Fig. 7. The healthy and damaged R spectrum plot of p1, p2, p12p, and p12s in Fig. 2c case of damage scenario.

connection in an enclosed rectangle. Fig. 11 shows an increasing trend of the RMSD damage index for added mass concerning the varying environmental temperature conditions. For the 5-g additional mass on the steel beam, the RMSD damage indices do not follow the same rising pattern as the p1, p2, and p12s cases. As a result, the p12p connection-based damage indices are best suited for detecting additional mass while having minimal influence on temperature change. The results suggest that connecting two transducers in parallel and conducting the measurement is sufficient, rather than measuring two transducers independently for damage detection.

Case II. The combinations of transducers were used to investigate a simulated crack at the left end of the beam, as shown in Fig. 2d. The temperature was increased from 19 °C to 24 °C and further to 31 °C to investigate the damage detection capability of the sensor arrangement. The abbreviations used for the healthy and damaged conditions in the analysis of crack damage detection are explained in Table 3.

Figs. 12–15 show an RMSD index-based study of the healthy and damaged state of the beam using EMI experimental R data. For the p1, p2, p12p, and p12s connections, the green bar shows the healthy state measurements at varying environmental temperatures and acts as a threshold to monitor damage presence. The RMSD damage index of p12p in the cracked beam case, illustrated by the red bar, is larger than the green bar, regardless of the healthy state values at varied external temperature conditions, as shown in Fig. 14. However, p1, p2, and p12s do not show such an increasing trend of RMSD damage index for the damage state, irrespective of the healthy state variation due to changing temperature conditions, as shown in Figs. 12, 13 and 15, respectively. In the simulated crack scenario, the p12p-based damage identification outperforms the performance of p1, p2, and p12s individually. Hence, the R-based RMSD damage indices are suitable for the investigation of

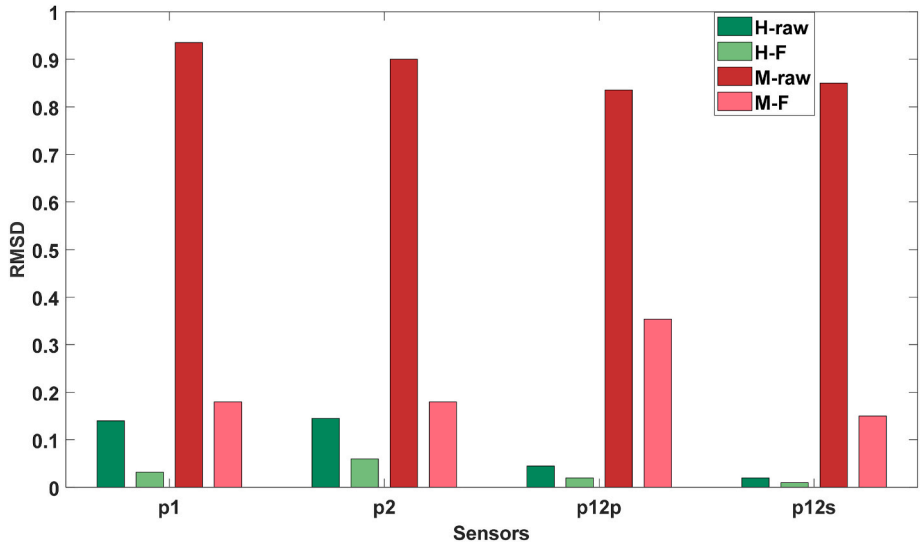

Fig. 8. The RMSD damage indices of the p1, p2, p12p, and p12s for raw and filtered spectra in the damage case, as shown in Fig. 2a.

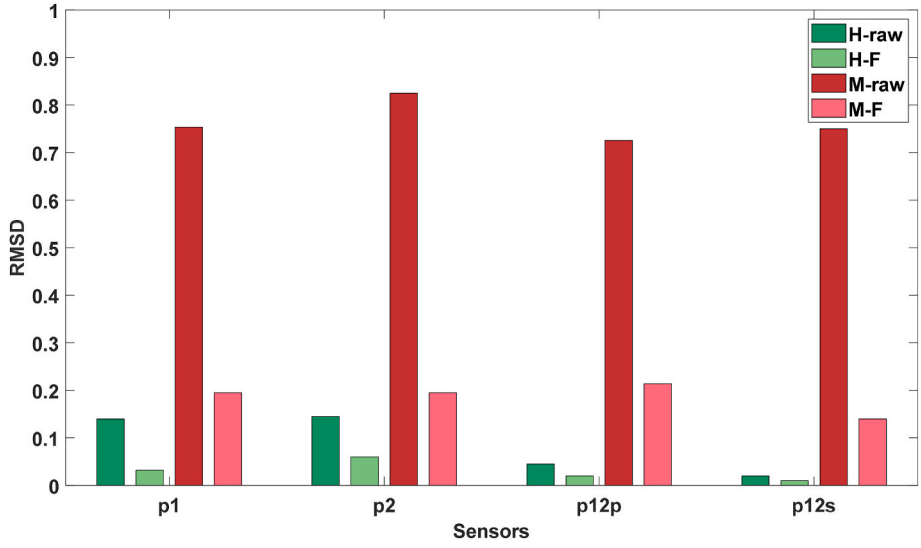

Fig. 9. The RMSD damage indices of the p1, p2, p12p, and p12s for raw and filtered spectra in the damage case, as shown in Fig. 2b.

the steel beam due to their lower sensitivity to temperature variation. The p12p connection reduces the resultant resistance amplitude from the p1 and p2, resulting in a lesser susceptibility to noise and the environment. Since the parallel connection uses the healthy and damaged states simultaneously for damage analysis. The damage index-based study is less affected by the deviation in the damage signal caused by variations in the temperatures. When connecting the combined signal in parallel, the output external effect resistance is smaller; when connecting in series, it is larger.

The damage detection investigation under varying temperature conditions consisted of two examples. In the first case study, a simulated very small mass is placed on the steel beam, whereas in the second case, a crack is simulated. In both situations, the damage was identified using a p12p connection. There are discrepancies in absolute values, but they do not affect the interpretation of the data. The p12p connections were less sensitive to temperature variations than the other individual and combined connections, although they could always detect damage. As a result, the p12p connection-based damage indices are effective in detecting additional weight and cracks for varying temperatures. Finally, we could decrease time consumption by employing the suggested connection for identifying masses in a variety of temperature settings.

5. Conclusions

Recent research has focused on lowering the size and cost of measurement instruments. For example, the AD5933 evaluation board was used for a bolt loosening test on a steel plate, to prove the method's feasibility and efficiency for identifying structural degradation [43]. However, effective damage detection in varying environmental temperature applications encourages novel piezo arrangements, which were previously limited to expediting the data retrieval process using the EMI method. This methodology broadened the scope of investigation of damage from individual transducers to fused connections to detect damage in temperature and noise precisely. The approach investigated parallel combinations and compared them to the output of individual transducers or series combinations for external temperature fluctuation. The damage index for the additional simulated mass and shallow cut (simulating a crack) on steel beams is investigated in this article under a few ambient temperature values. The damage sensitivity of a

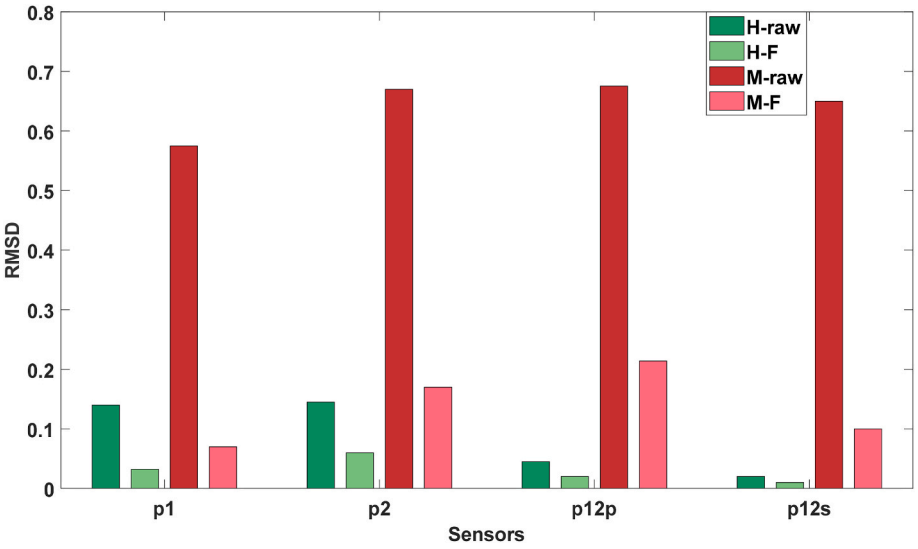

Fig. 10. The RMSD damage indices of the p1, p2, p12p, and p12s for raw and filtered spectra in the damage case, as shown in Fig. 2c.

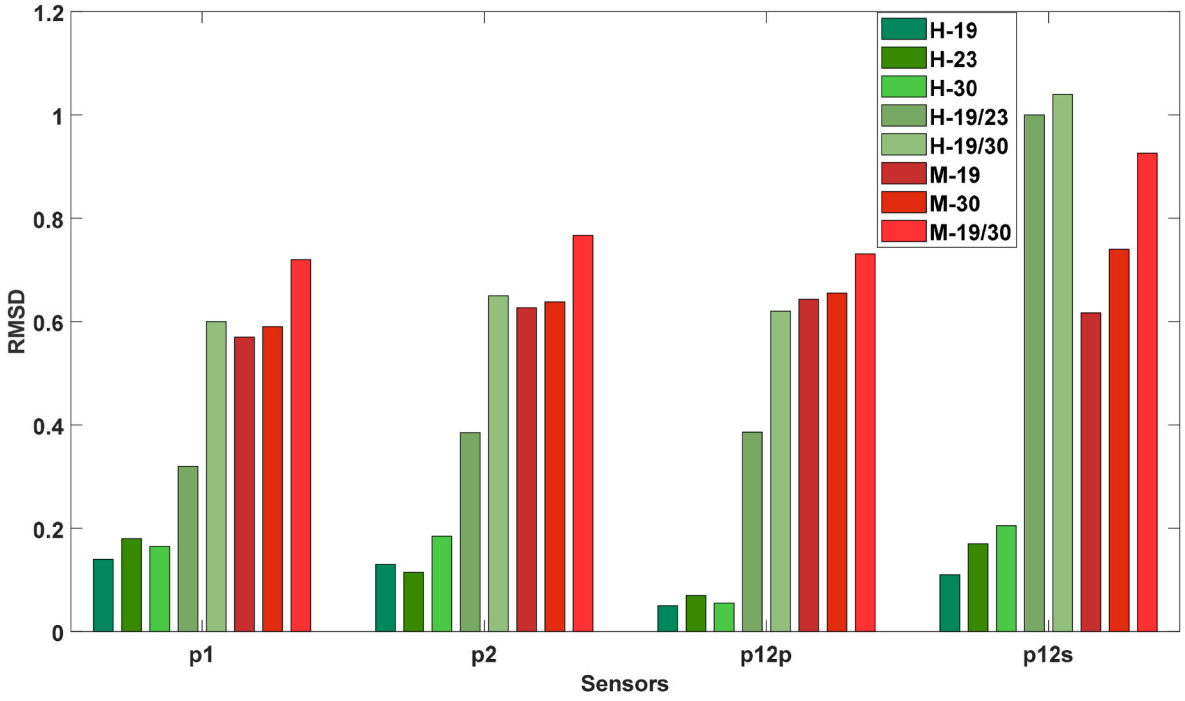

Fig. 11. The RMSD damage indices of p1, p2, p12p, and p12s in varying environmental temperature conditions for the damage case are shown in Fig. 2c.

Table 2
Used symbols and their explanations in the case of the added mass study.

H-19	Healthy at 19 °C with respect to (w.r.t) healthy at 19 °C
H-19/23	Healthy at 19 °C w.r.t healthy at 23 °C
H-19/30	Healthy at 19 °C w.r.t healthy at 30 °C
H-23	Healthy at 23 °C w.r.t healthy at 23 °C
H-30	Healthy at 30 °C w.r.t healthy at 30 °C
M-19	Added mass at 19 °C w.r.t healthy at 19 °C
M-30	Added mass at 30 °C w.r.t healthy at 30 °C
M-19/30	Added mass at 30 °C w.r.t healthy at 19 °C

multi-sensor parallel combination is compared. Furthermore, this article successfully represents the advantage of the fused resistance of two transducers based on parallel combinations utilizing RMSD, which has a lower sensitivity to noise and temperature variation in measurements.

The following benefits of parallel connections over single and series connections can be listed.

1. Combined resistance measurements using parallel sensors are approximately 50% faster than individual measurements of healthy and damaged states due to simultaneous data acquisition, as shown in Table 4.

2. The parallel configuration shows higher RMSD values for both small and large simulated damages (additional mass and shallow cuts), confirming improved sensitivity to structural degradation.
3. Parallel resistance measurements exhibit lower sensitivity due to reduced fluctuation under ambient temperature variation, demonstrating better stability compared to single and series configurations.

Table 3
Used symbols and their explanations in the case of the simulated crack study.

H19	Healthy at 19 °C w.r.t healthy at 19 °C
H19-24	Healthy at 19 °C w.r.t healthy at 24 °C
H19-31	Healthy at 19 °C w.r.t healthy at 31 °C
H24	Healthy at 24 °C w.r.t healthy at 24 °C
H24-31	Healthy at 24 °C w.r.t healthy at 31 °C
H31	Healthy at 31 °C w.r.t healthy at 31 °C
Dc19	Simulated crack at 19 °C w.r.t healthy at 19 °C
Dc24	Simulated crack at 24 °C w.r.t healthy at 19 °C
Dc31	Simulated crack at 31 °C w.r.t healthy at 19 °C
Dc19-24	Simulated crack at 19 °C w.r.t healthy at 24 °C
Dc19-31	Simulated crack at 19 °C w.r.t healthy at 31 °C
Dc24-31	Simulated crack at 24 °C w.r.t healthy at 31 °C
Dc24-19	Simulated crack at 24 °C w.r.t healthy at 19 °C
Dc31-19	Simulated crack at 31 °C w.r.t healthy at 19 °C
Dc31-24	Simulated crack at 31 °C w.r.t healthy at 24 °C

4. This study is important because it focuses on a simplified way of shortening measurement durations for the structure monitoring while also employing a resilient parallel connection method to explore damage sensitivity even in a temperature-varying environment.

Hence, the proposed parallel connection–based approach has been developed and validated primarily for flat structural specimens under controlled laboratory conditions. In the future, research will focus on developing parallel, larger subnetwork architectures for multi-damage localization and imaging in larger structures by enhancing the sensitivity range, thereby enhancing the scalability and practical applicability of the proposed method for damage detection in both metallic and composite materials. Moreover, efforts will be directed toward extending the parallel connection–based approach to curved and geometrically complex surfaces, where variations in electromechanical coupling present additional challenges.

CRediT authorship contribution statement

Shishir Kumar Singh: Writing – review & editing, Writing – original draft, Visualization, Validation, Software, Methodology, Investigation, Formal analysis, Data curation, Conceptualization. **Paweł H.**

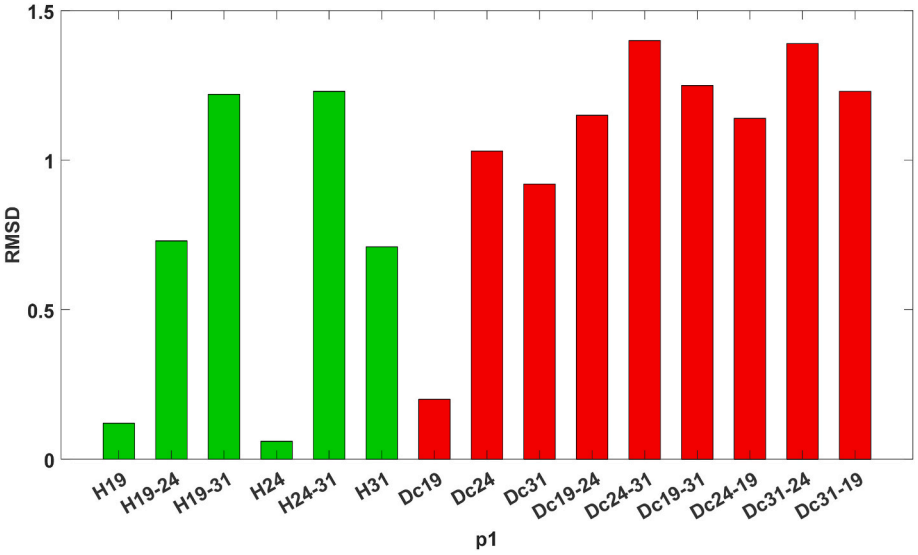

Fig. 12. The RMSD damage indices of p1 in varying temperature conditions for the developed crack in the beam.

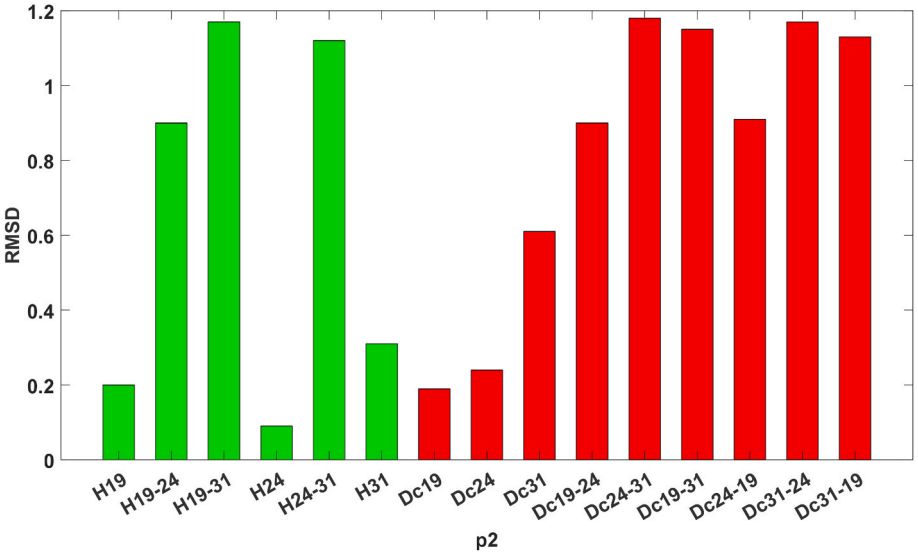

Fig. 13. The RMSD damage indices of p2 in varying temperature conditions for the developed crack in the beam.

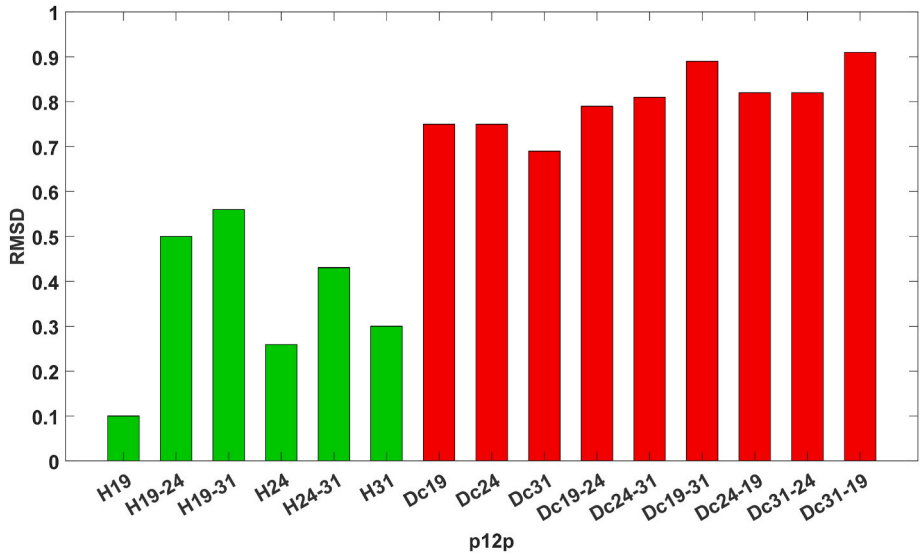

Fig. 14. The RMSD damage indices of p12p in varying temperature conditions for the developed crack in the beam.

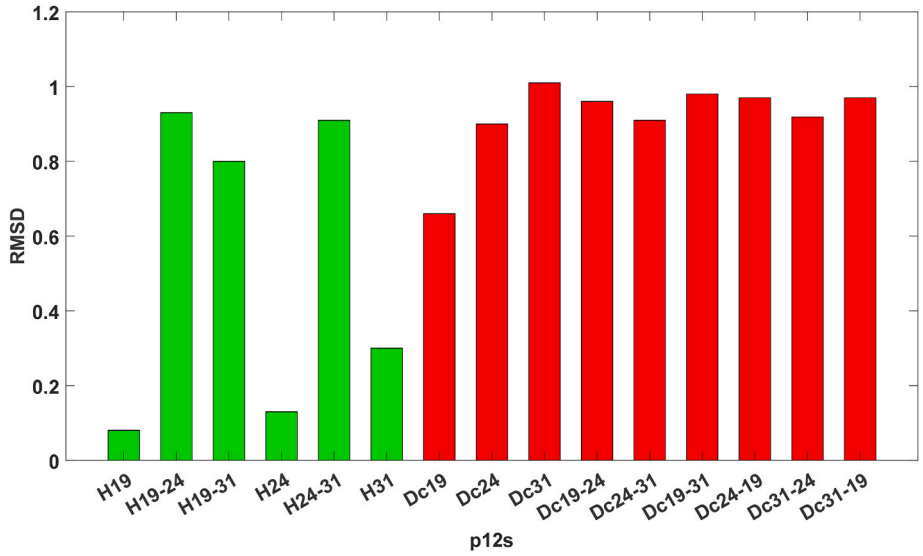

Fig. 15. The RMSD damage indices of p12s in varying temperature conditions for the developed crack in the beam.

Table 4
Comparative healthy and each damage scenario measurement speed for single, series, and parallel sensors.

Configuration	No. of Sensors Measured	Measurement Time (Healthy State)	Measurement Time (Damage State)	Relative Speed	Remarks
Two PZTs (measured individually)	2	2 × 46 min = 92 min	2 × 46 min = 92 min	1 ×	Total healthy baseline measurement time = 184 min Each damage scenario measurements time = 184 min
Two PZTs (Series connection)	2	46 min	46 min	2 × faster	Simultaneous baseline measurement time of both sensors = 92 min Each damage scenario measurements time = 92 min
Two PZTs (Parallel connection)	2	46 min	46 min	2 × faster	Simultaneous baseline measurement time = 92 min Each damage scenario measurements time = 92 min

Malinowski: Writing – review & editing, Supervision, Project administration, Funding acquisition, Conceptualization.

Declaration of competing interest

The authors declare that they have no known competing financial

interests or personal relationships that could have appeared to influence the work reported in this paper.

Acknowledgments

The funding support was provided by the National Science Center, Poland under the SONATA BIS project entitled: Study of piezoelectric sensors placement and their interaction with structural elements (2016/22/E/ST8/00068).

Data availability

Data will be made available on request.

References

[1] Baptista FG, Vieira Filho J. A new impedance measurement system for PZT-based structural health monitoring. IEEE Trans Instrum Meas 2009;58(10):3602–8.
[2] Wu J, Chen Y, Wang J, Liu Z, Li W. Electromechanical impedance instrumented wearable piezoelectric ring-type sensor for bolted connection monitoring. IEEE Sens J 2023;23(13):14872–81.
[3] Farrar CR, Park G, Allen DW, Todd MD. Sensor network paradigms for structural health monitoring. Struct Control Health Monit 2006;13(1):210–25. https://doi.org/10.1002/stc.125.
[4] Liang C, Sun F, Rogers CA. Electro-mechanical impedance modeling of active material systems. Smart Mater Struct 1996;5(2):171–86. https://doi.org/10.1088/0964-1726/5/2/006.
[5] Luo Z, Deng H, Li L, Luo M. A simple PZT transducer design for electromechanical impedance (EMI)-based multi-sensing interrogation. J Civil Struct Health Monit 2021;11(1):235–49. https://doi.org/10.1007/s13349-020-00449-6.
[6] Zuo C, Feng X, Zhang Y, Lu L, Zhou J. Crack detection in pipelines using multiple electromechanical impedance sensors. Smart Mater Struct 2017;26:aa7ef3. https://doi.org/10.1088/1361-665X/aa7ef3.
[7] Adhikari S, Bhalla S. Modified dual piezo configuration for improved structural health monitoring using electro-mechanical impedance (EMI) technique. Exp Tech 2019;43(1):25–40.
[8] Chen D, Huo L, Song G. EMI based multi-bolt looseness detection using series/parallel multi-sensing technique. Smart Struct Syst 2020;25:423–32.
[9] Singh SK, Ostachowicz WM, Malinowski PH. Damage study using series and parallel electrode in electromechanical impedance method. In: Rizzo P, Milazzo A, editors. EWSHM 2020. Lecture Notes in Civil Engineering, 128. Cham: Springer; 2021. p. 1–9. https://doi.org/10.1007/978-3-030-64908-1_75.
[10] Bharathi Priya C, Jothi Saravanan T, Balamonica K, et al. EMI based monitoring of early-age characteristics of concrete and comparison of serial/parallel multisensing technique. Constr Build Mater 2018;191:1268–84.
[11] K B, T JS, C BP, N G. Piezoelectric sensor–based damage progression in concrete through serial/parallel multi-sensing technique. Struct Health Monit 2020;19(2):339–56. https://doi.org/10.1177/1475921719845153.
[12] Krishnamurthy K, Lalande F, Rogers CA. Effects of temperature on the electrical impedance of piezoelectric sensors. In: Proc SPIE smart structures and materials 1996: smart structures and integrated systems, San Diego, CA, 2717; 1996.
[13] Lim HJ, Kim MK, Sohn H, Park CY. Impedance based damage detection under varying temperature and loading conditions. Ndt & E International 2011;44(8):740–50.
[14] Park G, Kabeya K, Cudney HH, et al. Impedance-based structural health monitoring for temperature varying applications. JSME Int J Ser A Solid Mech Mater Eng 1999;42(2):249–58.
[15] Wandowski T, Malinowski PH, Ostachowicz WM. Temperature and damage influence on electromechanical impedance method used for carbon fibre-reinforced polymer panels. J Intell Mater Syst Struct 2017;28(6):782–98.
[16] Sun FP, Chaudhry ZA, Rogers CA, et al. Automated real-time structure health monitoring via signature pattern recognition. In: Proc SPIE smart structures and materials 1995: smart structures and integrated systems, San Diego, CA, 2443; 1995.
[17] Li H, Ai D, Zhu H, Luo H. Integrated electromechanical impedance technique with convolutional neural network for concrete structural damage quantification under varied temperatures. Mech Syst Signal Process 2021;152:107467.
[18] Ai D, Mo F, Cheng J, Du L. Deep learning of electromechanical impedance for concrete structural damage identification using 1-D convolutional neural networks. Constr Build Mater 2023;385:131423.
[19] Sapidis GM, Naoum MC, Papadopoulos NA, Golias E, Karayannis CG, Chalioris CE. A novel approach to monitoring the performance of carbon-fiber-reinforced polymer retrofitting in reinforced concrete beam–column joints. Applied Sciences 2024;14(20):9173.
[20] Sapidis GM, Naoum MC, Papadopoulos NA. Electromechanical impedance-based compressive load-induced damage identification of fiber-reinforced concrete. Infrastructures 2025;10(3):60.
[21] Mirgal P, del-Río-Velilla D, Wandowski T, Majewska K, Malinowski PH. Temperature-driven changes in electromechanical impedance technique applied for damage detection in 3D printed plates. In: Health monitoring of structural and biological systems XIX, 13437. SPIE; 2025, May. p. 287–92.
[22] Huang X, Qu W, Xiao L. Temperature compensation method for impedance signals of bolt loosening under temperature varying conditions using TransUnet. Smart Mater Struct 2024;33(10):105035.
[23] Zhao S, Fan S, Yang J, Kitipornchai S. Numerical and experimental investigation of electro-mechanical impedance based concrete quantitative damage assessment. Smart Mater Struct 2020;29(5):055025.
[24] Zhao S, Fan S, Yang J, Kitipornchai S. A spherical smart aggregate sensorbased electro-mechanical impedance method for quantitative damage evaluation of concrete. Struct Health Monit 2019;19(5):1560–76.
[25] Zhu J, Qing X, Liu X, Wang Y. Electromechanical impedance-based damage localization with novel signatures extraction methodology and modified probability-weighted algorithm. Mech Syst Signal Process 2021;146:107001.
[26] Na WS, Baek J. A review of the piezoelectric electromechanical impedance based structural health monitoring technique for engineering structures. Sensors (Basel) 2018;18(5):1307. https://doi.org/10.3390/s18051307.
[27] Peairs DM, Tarazaga PA, Inman DJ. Frequency range selection for impedance-based structural health monitoring. 2007.
[28] Rao RK, Sasmal S. Electromechanical impedance-based embeddable smart composite for condition-state monitoring. Sensor Actuator Phys 2022;346:113856.
[29] Qing XP, Beard SJ, Kumar A, Ooi TK, Chang FK. Built-in sensor network for structural health monitoring of composite structure. J Intell Mater Syst Struct 2007;18(1):39–49.
[30] Singh SK, Andrearczyk A, Malinowski PH. Damage detection in 3D-printed plate using the electromechanical impedance method with surface bonded and embedded sensors. In: Health monitoring of structural and biological systems XVIII, 12951. SPIE; 2024. p. 195–200.
[31] Gomasa R, Talakokula V, Jyosyula SKR, Bansal T. Strength monitoring and prediction of blended concrete systems from very early to delayed Age using embedded Piezo sensor data: an experimental and machine learning approach. J Build Eng 2025:112677.
[32] Naoum Maria C, Papadopoulos Nikos A, Sapidis George M, Voutetaki Maristella E. Efficacy of PZT sensors network different configurations in damage detection of fiber-reinforced concrete prisms under repeated loading. Sensors 2024;24(17):5660.
[33] Baptista FG, Vieira Filho J. Optimal frequency range selection for PZT transducers in impedance-based SHM systems. IEEE Sens J 2010;10(8):1297–303.
[34] Singh SK, Malinowski PH. An innovative data-driven probabilistic approach for damage detection in electromechanical impedance technique. Compos Struct 2022;295:115808.
[35] Singh SK, Fakih MA, Malinowski PH. Damage detection and localization based on different types of actuators using the electromechanical impedance method in 3D-printed material. Smart Mater Struct 2023;32(11):115004.
[36] Press WH, Saul AT. Savitzky-Golay smoothing filters. Comput Phys 1990;4(6):669. https://doi.org/10.1063/1.4822961.
[37] Skarbek L, Wandowski T, Opoka S, Malinowski P, Ostachowicz W. Electromechanical impedance technique and scanning vibrometry for structure characterization. In: Proc 6th European workshop on structural health monitoring, 1; 2012. p. 179–85.
[38] Kim J, Grisso BL, Kim JK, Ha DS, Inman DJ. Electrical modeling of piezoelectric ceramics for analysis and evaluation of sensory systems. In: 2008 IEEE sensors applications symposium. IEEE; 2008. p. 122–7.
[39] Van Dyke KS. The piezo-electric resonator and its equivalent network. Proc Inst Radio Eng 1928;16(6):742–64.
[40] Guan M, Liao WH. Studies on the circuit models of piezoelectric ceramics. In: International Conference on Information Acquisition, 2004. Proceedings. IEEE:—frequency range citation; 2004. p. 26–31.
[41] Singh SK, Fakih MA, Malinowski P. A sensitivity study of different actuators for the electromechanical impedance method in 3D-printed material. In: European workshop on structural health monitoring. Cham: Springer International Publishing; 2022, June. p. 874–82.
[42] https://www.imp.gda.pl/fileadmin/doc/BIP/postepowania_o_nadanie_stopnia_doktora/Shishir_Singh/Thesis_Singh.pdf.
[43] Tan Z, Feng Q, Ma T, Zhang J, Liang Y. Development of an AD5933-based impedance calibration and measurement technology using piezoceramic transducers. Measurement 2023;210:112527.